

Fitting for the energy levels of hydrogen

David M. Jacobs*

*Physics Department, Norwich University, Northfield, Vermont 05663, USA and
Physics Department, Case Western Reserve University, Cleveland, Ohio 44106, USA*

Marko Horbatsch†

Department of Physics and Astronomy, York University, Toronto, Ontario, Canada M3J 1P3

(Dated: August 29, 2023)

Atomic hydrogen energy levels calculated to high precision are required to assist experimental researchers working on spectroscopy in the pursuit of testing quantum electrodynamics (QED) and probing for physics beyond the Standard Model. There are two important parts to the problem of computing these levels: an accurate evaluation of contributions from QED and using an accurate value for the proton charge radius as an input. Recent progress on QED corrections to the fine structure, as well as increasing evidence that a proton charge radius in the range of 0.84 fm is favored over the previously adopted larger value in the 0.88 fm range, has advanced the field, yet several state-of-the-art measurements remain in contradiction with this smaller value. Motivated by on-going and future work in this area, we present here a simple parameterization for the energy levels of hydrogen at the level of hyperfine structure using the so-called relativistic Ritz approach. The fitting of a finite sample of QED-generated levels at low to intermediate principal quantum number, n , gives a generally applicable formula for *all* values of n for each distinct angular momentum channel, given in this work up to orbital angular momentum number $\ell = 30$. We also provide a simple linear parameterization for the shift in hydrogen energy levels as a function of the proton radius, providing a useful cross check for extant and future measured energy intervals.

I. INTRODUCTION

Precision measurements of atoms are used for metrological purposes and testing the theory of quantum electrodynamics (QED). This is of current interest also in the context of beyond-the-Standard-Model phenomena, as they could manifest themselves in atomic spectroscopy [1]. The theory of bound-state QED is sufficiently mature that the dominant uncertainty in its predictions for the levels of hydrogen and deuterium is due to the nuclear radius. The proton radius puzzle first appeared in 2010 [2] when muonic hydrogen measurements indicated that r_p is 4% smaller than had been previously determined, a value near 0.88 fm [3]. Over the last decade or so, more scattering and spectroscopic experiments have been performed that suggest a value of r_p closer to 0.84 fm [4]. However, discrepancies remain, such as the results of Fleurbaey et al. [5] and Brandt et al. [6], that indicate a value of r_p larger than 0.84 fm with substantial statistical significance. Thus, the puzzle is not entirely solved; more measurements are planned in the near future, including that of the $1S_{1/2} \rightarrow 4S_{1/2}$ interval [7].

The bound-state QED predictions for the energy levels of hydrogen involve a combination of long analytic expressions and numerical results that are cumbersome to

use; see, e.g., [8]. Our goal here is to provide a fitting formula that reproduces the bound-state QED predictions for those energy levels to sufficiently high accuracy that bound-state QED need not be used directly. To this end, we use the so-called relativistic Ritz approach, which is a long-distance effective theory describing the bound states of two-particle systems whose binding potential is dominated by the Coulomb interaction [9]. In that effective theory, the energy levels of atomic hydrogen were shown to be

$$\frac{E}{c^2} = \sqrt{m_e^2 + m_p^2 + \frac{2m_e m_p}{\sqrt{1 + \left(\frac{\alpha}{n_\star}\right)^2}}} - (m_e + m_p), \quad (1)$$

where α is the fine-structure constant and the effective quantum number

$$n_\star = n - \delta. \quad (2)$$

The quantum defect, δ , itself depends on the principal quantum number, n , and accounts for interactions that are shorter in range than the Coulomb interaction; it also depends on the orbital, total electronic, and total system quantum numbers, ℓ , j , and f , respectively.

To make the numerical analyses more efficient, we Taylor expand equation (1) in small α up to eighth order¹

* david.m.jacobs@asu.edu; Present Address: Department of Physics, Arizona State University, Tempe, AZ 85281

† marko@yorku.ca

¹There is no ninth order term so this is sufficient for the accuracy required here. Furthermore, the highest computed QED terms have so far not been computed at higher precision than this [8].

and factor out the Rydberg frequency,

$$cR_\infty \equiv \frac{m_e \alpha^2 c^2}{2h}, \quad (3)$$

allowing us to write

$$\frac{E}{h} = cR_\infty \left(\frac{A_2}{n_*^2} + \frac{A_4}{n_*^4} + \frac{A_6}{n_*^6} + \frac{A_8}{n_*^8} \right), \quad (4)$$

where the $A_{2k} = \mathcal{O}(\alpha^{2k-2})$. For the value of the fine-structure constant we use

$$\alpha^{-1} = 137.035\,999\,166(15), \quad (5)$$

derived from a recent measurement of the electron g-factor [10]. Together with the mass ratio

$$\frac{m_p}{m_e} = 1\,836.152\,673\,349(71), \quad (6)$$

inferred from spectroscopy of HD^+ [11]², this allows us to determine the constants

$$A_2 = -0.999\,455\,679\,424\,739(21) \quad (7)$$

$$A_4 = 3.990\,953\,7921(87) \times 10^{-5} \quad (8)$$

$$A_6 = -1.770\,774 \times 10^{-9} \quad (9)$$

$$A_8 = 8.25 \times 10^{-14}. \quad (10)$$

There are uncertainties in A_6 and A_8 ; however, they are irrelevant at the level of accuracy needed here.

The simplest Ritz-like expansion is posited for the quantum defect, namely a series expansion in terms of the energy eigenvalues, which are assumed to be small relative to some high-energy scale, Λ :

$$\delta = \delta_0 + \lambda_1 \frac{E}{\Lambda} + \lambda_2 \left(\frac{E}{\Lambda} \right)^2 + \dots, \quad (11)$$

where δ_0 and the λ_i are dimensionless coefficients. However, because in this form E depends implicitly on δ , it is impractical to use for most theoretical or empirical applications. A *modified* ansatz written as a series in inverse powers of $(n - \delta_0)$ is asymptotically ($n \rightarrow \infty$) equivalent to (11) and is significantly easier to use for data fitting. Analyzing the large- n behavior of (4) with (11), it may be verified that

$$\begin{aligned} \delta = \delta_0 &+ \frac{\delta_2}{(n - \delta_0)^2} + \frac{\delta_4}{(n - \delta_0)^4} + \frac{2\delta_2^2}{(n - \delta_0)^5} + \frac{\delta_6}{(n - \delta_0)^6} + \frac{6\delta_2\delta_4}{(n - \delta_0)^7} + \frac{\delta_8}{(n - \delta_0)^8} + \frac{4\delta_4^2 + 8\delta_2\delta_6}{(n - \delta_0)^9} \\ &+ \frac{\delta_{10}}{(n - \delta_0)^{10}} + \frac{-40\delta_2^4 + 10\delta_4\delta_6 + 10\delta_2\delta_8}{(n - \delta_0)^{11}} + \frac{\delta_{12}}{(n - \delta_0)^{12}} + \frac{-296\delta_2^3\delta_4 + 6\delta_6^2 + 12\delta_4\delta_8 + 12\delta_2\delta_{10}}{(n - \delta_0)^{13}} + \dots, \quad (12) \end{aligned}$$

where the δ_i are free parameters. As shown in the following section, δ_0 is small (of order α^2) and thus $1/(n - \delta_0)$ is small for $n > 1$, but we find that the modified defect expansion (12) satisfactorily reproduces energy levels even for $n = 1$ with the inclusion of a sufficient number of δ_i .

A truncation of equation (12) is required for any application and we specify the order of the analysis by the highest inverse power of $(n - \delta_0)$ included. Actually, truncations made at each successive inverse *odd* power includes one additional defect parameter. Because there is no -1 st or -3 rd term, including terms through $(n - \delta_0)^{-1}$

requires only δ_0 and is considered lowest order (LO), whereas including terms through $(n - \delta_0)^{-3}$ requires both δ_0 and δ_2 and is considered next-to-lowest order (NLO). At higher orders we use the abbreviation N^kLO , where $k + 1$ is equal to the number of defect parameters needed. For practical purposes, as shown below, the largest expansion is needed for S -states, where we truncate at the level N^6LO , thereby including defect parameters up to δ_{12} . For higher angular momentum eigenstates fewer terms are required to reach the same level of accuracy.

As outlined below, we use a limited number of precisely calculated energy levels of hydrogen employing the most up-to-date bound-state QED calculations [8], and fit them with equation (4) using the defect formula in equation (12). We determine the necessary δ_i to reproduce all theoretical energy levels to within their uncertainties and demonstrate the power of our fits by testing

²This value is consistent with that of Ref. [12]. Both values reported in Refs. [11] and [12] rely on the proton-to-deuteron mass ratio obtained by Fink and Myers [13].

our results against higher- n calculated energies. Because some energies can be predicted with a relative precision that is better than 10^{-13} , to ensure this level of reproducibility, the parameters A_2 through A_8 are given to an absolute precision of 10^{-15} and, likewise, we report our fit values of the δ_i to the same level of precision.

II. THEORETICAL INPUTS, UNCERTAINTIES, AND SHIFTS DUE TO THE PROTON RADIUS

According to bound-state QED, the theoretical energy levels of hydrogen can be written as the sum of a gross level structure, fine-structure (FS), and hyperfine-structure (HFS) contribution,

$$E_{n\ell j f} = -\frac{cR_\infty}{n^2} \frac{m_p}{m_p + m_e} + E_{n\ell j}^{(\text{FS})} + E_{n\ell j f}^{(\text{HFS})}, \quad (13)$$

where we have chosen units in which Planck's constant, $\hbar = 1$. The electron's reduced Compton wavelength, muon-to-electron mass ratio, proton g-factor, and electron magnetic-moment anomaly taken from CODATA-18 [8] are

$$\lambda_e = 3.861\,592\,6796(12) \times 10^{-13} \text{ m} \quad (14)$$

$$\frac{m_\mu}{m_e} = 206.768\,2830(46) \quad (15)$$

$$g_p = 5.585\,694\,6893(16) \quad (16)$$

$$a_e = 1.159\,652\,181\,28(18) \times 10^{-3}. \quad (17)$$

We also use the proton radius inferred from the muonic hydrogen spectroscopy of Antognini et al. 2013 [14],

$$r_p = 0.840\,87(39) \text{ fm}. \quad (18)$$

Following the procedure described in [15], the measured $1S_{1/2}$ [16] and $2S_{1/2}$ [17] hyperfine intervals may be used to determine $E_{n\ell j f}^{(\text{HFS})}$ to sufficient accuracy such that cR_∞ may be determined using the measured $1S_{1/2}^{(f=1)} \rightarrow 2S_{1/2}^{(f=1)}$ interval from [18]; this completely specifies the theory.

The theoretical uncertainty in the energy levels is dominated by the uncertainty in $E_{n\ell j}^{(\text{FS})}$, which affects the levels directly through $E_{n\ell j}^{(\text{FS})}$ itself and also indirectly through the determination of cR_∞ . There are 5 uncertainties relevant to $E_{n\ell j}^{(\text{FS})}$ at the level of precision needed in this work. Four of these are QED uncertainties taken directly from CODATA-18 [8]: the uncertainty in the two-photon correction term B_{60} yields $\delta_{\ell,0} (0.94 \text{ kHz})/n^3$ (a reduction by about 50% compared to CODATA-14); the uncertainty in the three-photon correction term C_{50} yields $\delta_{\ell,0} (0.96 \text{ kHz})/n^3$; nuclear polarizability uncertainty yields $\delta_{\ell,0} (0.39 \text{ kHz})/n^3$; and a radiative recoil uncertainty yields $\delta_{\ell,0} (0.74 \text{ kHz})/n^3$.

In addition to the QED uncertainties mentioned above, there is an error in $E_{n\ell j}^{(\text{FS})}$ due to the proton radius (18)

which amounts to $\delta_{\ell,0} (1.03 \text{ kHz})/n^3$. Adding all of these errors in quadrature, the overall uncertainty in the fine-structure correction is

$$\delta(E_{n\ell j}^{(\text{FS})}) = \frac{(1.9 \text{ kHz})}{n^3} \delta_{\ell,0}, \quad (19)$$

and it follows that

$$cR_\infty = 3\,289\,849\,602\,49.1(2.2) \text{ kHz}, \quad (20)$$

a shift upward of 0.2 kHz compared to the result reported in [15], but well within the uncertainty computed therein. Accounting for the correlated uncertainties in the QED predictions and determination of cR_∞ , the theoretical uncertainty on any given level is

$$\delta(E_{n\ell j f}) = \left| \frac{1.9 \text{ kHz}}{n^3} \delta_{\ell,0} - \frac{2.2 \text{ kHz}}{n^2} \right|, \quad (21)$$

and is therefore below 0.6 kHz for all levels.

Lastly, given the potential issue of a remaining proton radius puzzle, we consider the possible systematic implications of a shift away from the value quoted in equation (18). Defining the proton radius shift,

$$\Delta r_p = r_p - 0.840\,87 \text{ fm}, \quad (22)$$

it follows that the Rydberg frequency shifts by

$$\Delta(cR_\infty)_{r_p} = 3.1 \text{ kHz} \left(\frac{\Delta r_p}{0.001 \text{ fm}} \right), \quad (23)$$

and the energy levels shift by

$$\Delta(E_{n\ell j f})_{r_p} = \left(\frac{2.6 \text{ kHz}}{n^3} \delta_{\ell,0} - \frac{3.1 \text{ kHz}}{n^2} \right) \left(\frac{\Delta r_p}{0.001 \text{ fm}} \right). \quad (24)$$

Equations (23) and (24) will be utilized below to cross check our results against a selection of experimental results.

III. FITTING TO THEORETICAL LEVELS OF HYDROGEN

A. Overview

For a given orbital angular momentum value, ℓ , we generate values of $E_{n\ell j f}$ using (13), following the same procedure described in Ref. [15] with updated theoretical inputs from Ref. [8]. Values of Bethe logarithms are taken from Refs. [19] and [20]; however, many levels require numerically-computed QED terms, such as $B_{60}(n\ell j)$, which have not been computed (or made publicly available) for all values of n , ℓ , and j . Therefore, we fit the available values of such terms with simple formulas in terms of inverse powers of n and interpolate or extrapolate to obtain the needed terms. Our conservative estimates for the interpolation/extrapolation error is far below the theoretical (QED) error.

We compute energy levels from $n_{\min} = \ell + 1$ up to $n_{\max} = \max(15, \ell + 1)$, fit them with equation (4) using the defect formula in equation (12), and weight each data point by the inverse square of the theoretical uncertainty given in (21). The fit order, i.e. the number of necessary defect parameters (δ_i), is increased until the difference between the fit value and the QED value from (13) falls below the QED error given in equation (21). Some example fits for a subset of $\ell = 0$ and $\ell = 1$ states are shown in Figures 1 and 2, which show the absolute differences between the relativistic Ritz and QED predictions; differences that do not appear in the figures are below 1 Hz. For these states, we have used QED-predicted levels up to $n_{\max} = 15$ for the fits, so all $n > 15$ values represent a true test of the model against QED.

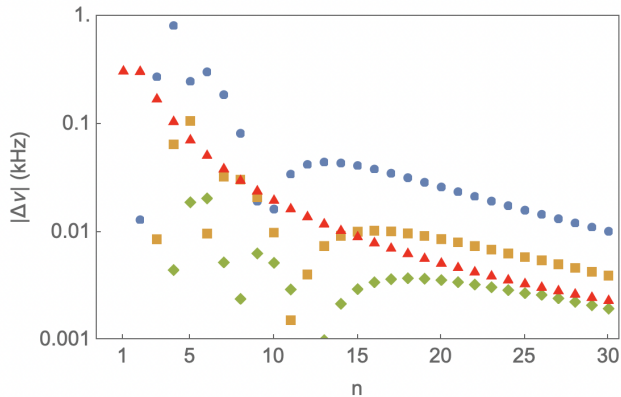


FIG. 1: Absolute differences between fit values of the energy levels from equation (4) and QED theory from equation (13) for $S_{j=1/2}^{(f=1)}$ states. The N^4 LO, N^5 LO, and N^6 LO fit differences are indicated by solid circles, squares, and diamonds, respectively, while the QED theory error is indicated with solid triangles.

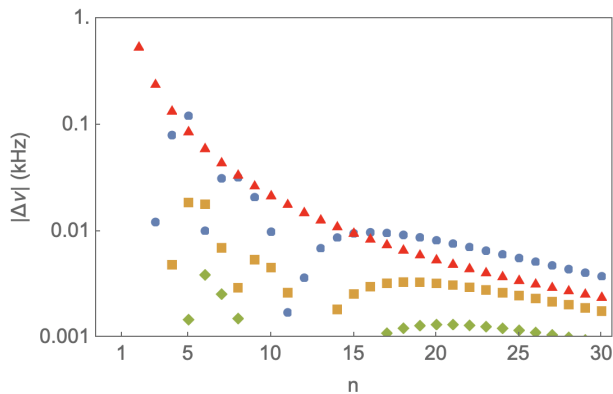


FIG. 2: Same as in Figure 1 but for $P_{j=3/2}^{(f=1)}$.

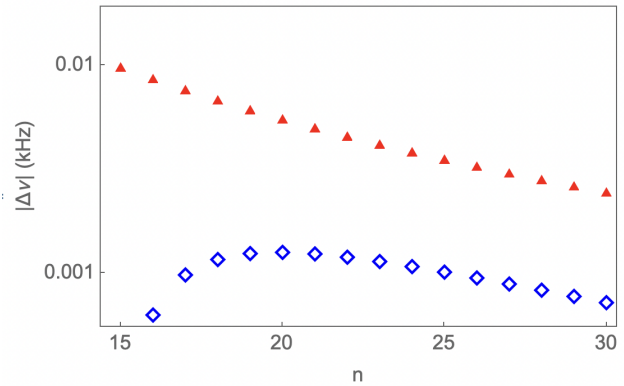


FIG. 3: Analogous to Figure 1 but for $\ell = 14$, $j = 29/2$, and $f = 15$. Open diamonds indicate differences for the LO fit, while solid triangles indicate the QED theory error. Notably, only one QED-predicted level ($n = 15$) was used to fit for δ_0 .

Summarizing the findings presented in Figs. 1 and 2 we make the following observations: The number of fit parameters required, i.e., the order of the expansion in (12) depends on the angular momentum value ℓ . This is related physically to the fact that states with $\ell > 0$ have a centrifugal barrier preventing the electron from getting close to the proton. For S -states the complete model as written out in (12) is required, and with increasing integer values of ℓ the required order tends to decrease until $\ell = 9$, beyond which only δ_0 is needed. This trend is partially demonstrated in Fig. 1, where $\ell = 0$ and the N^6 LO model provides an adequate fit, while in Fig. 2 ($\ell = 1$) the N^5 LO model is shown to provide sufficient accuracy. In either case, the low- n levels are reproduced with such precision (< 1 Hz) that they do not appear in the figures.

The full set of fit parameters for $\ell = 0$ and $\ell = 1$ states is shown in Table I, and Tables V - VIII in Appendix A present fit parameters for states from $\ell = 2$ to $\ell = 30$. The number of fit parameters for each combination of ℓ, j , and f never exceeds the number of energy values used for each fit. In fact, for states with $\ell \geq 14$ we have only used one QED-predicted level to fit for the one defect parameter (δ_0) required and have verified our model predictions up to at least $n = 30$; see Fig. 3 for an example in which $\ell = 14$. This points to the efficiency of the relativistic Ritz family of models.

We observe in Table I and Tables V - VIII that the behavior of the leading-order defect parameter, δ_0 , displays a strong dependence on j , a weak dependence on ℓ , and an even weaker dependence on f . The scale and variation of δ_0 can be understood from the following simplified non-relativistic analysis with fine- and hyperfine structure corrections included. In the $m_e/m_p \rightarrow 0$ limit,

ℓ	j	f	δ_i	Value/ 10^{-5}
0	$\frac{1}{2}$	0	δ_0	2.550 210 0611
			δ_2	0.008 375 5621
			δ_4	-0.031 662 6562
			δ_6	0.271 465 6639
			δ_8	-1.493 445 3489
			δ_{10}	3.605 726 0079
			δ_{12}	-2.356 090 4800
0	$\frac{1}{2}$	1	δ_0	2.528 610 1667
			δ_2	0.008 375 3687
			δ_4	-0.031 651 9458
			δ_6	0.271 324 9311
			δ_8	-1.492 530 9405
			δ_{10}	3.603 313 0305
			δ_{12}	-2.354 461 9943
1	$\frac{1}{2}$	0	δ_0	2.669 249 8201
			δ_2	0.002 680 7904
			δ_4	-0.023 483 8927
			δ_6	0.234 141 1690
			δ_8	-1.259 283 0776
			δ_{10}	2.428 620 8124
1	$\frac{1}{2}$	1	δ_0	2.662 051 7448
			δ_2	0.002 681 1814
			δ_4	-0.023 484 0422
			δ_6	0.234 143 0659
			δ_8	-1.259 294 3395
			δ_{10}	2.428 643 5695
1	$\frac{3}{2}$	1	δ_0	1.331 250 5239
			δ_2	0.002 680 3758
			δ_4	-0.023 507 0995
			δ_6	0.234 315 4776
			δ_8	-1.259 730 2288
			δ_{10}	2.428 830 0568
1	$\frac{3}{2}$	2	δ_0	1.328 373 2345
			δ_2	0.002 680 4364
			δ_4	-0.023 507 0852
			δ_6	0.234 315 3010
			δ_8	-1.259 729 2077
			δ_{10}	2.428 828 0568

TABLE I: Relativistic Ritz fitting parameters for $\ell = 0$ and $\ell = 1$ HFS states of hydrogen. Note that the numbers are small, since they are to be multiplied by 10^{-5} . For states with $2 \leq \ell \leq 30$ see Appendix A.

we can approximate

$$\begin{aligned} \frac{E}{h} &\simeq -\frac{cR_\infty}{(n - \delta_0)^2} \\ &\simeq -cR_\infty \left(\frac{1}{n^2} + \frac{2}{n^3} \delta_0 \right), \end{aligned} \quad (25)$$

where in the second line we have assumed $\delta_0/n \ll 1$, which is verified below. It is well known that fine-structure effects contribute to the energy levels a j -

dependent term that scales³ as n^{-3} ,

$$\Delta E^{(\text{FS})} = -\frac{cR_\infty}{n^3} \frac{\alpha^2}{j + 1/2} + \dots, \quad (26)$$

so we should expect that

$$\delta_0 \simeq \frac{\alpha^2}{2j + 1}. \quad (27)$$

Hyperfine structure effects contribute to the energy a leading term (see, e.g., [15]) that is approximately

$$\Delta E^{(\text{HFS})} \simeq \begin{cases} 1.42 \text{ GHz} \times \frac{(f - \frac{3}{4})}{n^3} & (\ell = 0) \\ 0.53 \text{ GHz} \times \frac{f(f+1) - j(j+1) - \frac{3}{4}}{n^3(2\ell+1)j(j+1)} & (\ell \neq 1), \end{cases} \quad (28)$$

which means that we should expect deviations in the leading order defect due to HFS effects (at fixed ℓ and j) that are approximately

$$\Delta(\delta_0)_{\text{HFS}} \simeq \begin{cases} 2.2 \times 10^{-7} & (\ell = 0) \\ 8.1 \times 10^{-8} \times j^{-2} & (\ell \gg 1). \end{cases} \quad (29)$$

This accounts for the approximate differences between the δ_0 as seen in Table I as well as for the rest of the angular momentum channels, up to $\ell = 30$, listed in Tables V - VIII in Appendix A.

We should, however, point out that the precise values for the defect parameters depend somewhat on which QED-predicted levels are used for the fit. For the states of low-lying ℓ we have chosen $n_{\text{max}} = 15$, but as an example we reconsider the $S_{j=1/2}^{(f=0)}$ states by fitting to levels up to $n_{\text{max}} = 16$. A comparison of the parameters between the $n_{\text{max}} = 15$ and $n_{\text{max}} = 16$ fits are shown in Table II. Minor changes in δ_0 are observed, but more substantial changes are seen for the higher-order parameters. Nevertheless, either set of parameters could be used to reproduce the QED-predicted energy levels at a comparable level of accuracy.

Parameter	$n_{\text{max}} = 15$ ($\times 10^{-5}$)	$n_{\text{max}} = 16$ ($\times 10^{-5}$)
δ_0	2.5502100611	2.5502099872
δ_2	0.0083755621	0.0083855869
δ_4	-0.0316626562	-0.0320835870
δ_6	0.2714656639	0.2786622804
δ_8	-1.4934453489	-1.5454747300
δ_{10}	3.6057260079	3.7472037620
δ_{12}	-2.3560904800	-2.4523221495

TABLE II: Comparison of fitting parameters for $S_{j=1/2}^{(f=0)}$ states between the $n_{\text{max}} = 15$ and $n_{\text{max}} = 16$ fit.

³The fine-structure correction that scales as n^{-4} is a relativistic kinetic energy correction that is already contained within the relativistic Ritz model – see equation (4).

Some comments on this procedure are warranted. The defect parameters, δ_i , are perhaps best viewed as parameters of a particular fitting function, which is not unique, applied to a particular set of input data, which also is not unique. In fact, there are strong correlations between the parameters; see Table III for the correlation matrix between defect parameters for the $S_{j=1/2}^{(f=0)}$ fit. Therefore,

TABLE III: Correlation Matrix for the $S_{j=1/2}^{(f=0)}$ fit.

	δ_0	δ_2	δ_4	δ_6	δ_8	δ_{10}	δ_{12}
δ_0	1.00000	-0.94504	0.88620	-0.84558	0.82121	-0.80876	0.80445
δ_2	-0.94504	1.00000	-0.98466	0.96259	-0.94653	0.93770	-0.93456
δ_4	0.88620	-0.98466	1.00000	-0.99480	0.98747	-0.98274	0.98097
δ_6	-0.84558	0.96259	-0.99480	1.00000	-0.99838	0.99641	-0.99557
δ_8	0.82121	-0.94653	0.98747	-0.99838	1.00000	-0.99961	0.99930
δ_{10}	-0.80876	0.93770	-0.98274	0.99641	-0.99961	1.00000	-0.99996
δ_{12}	0.80445	-0.93456	0.98097	-0.99557	0.99930	-0.99996	1.00000

B. Comparison with experiments

As an example application of these fits, in Table IV we provide a selection of recently measured hydrogen transition frequencies and their corresponding theory predictions using equation (4). Weighting by the number of states, the hyperfine centroid is defined as

$$E_{n\ell j}^{\text{centroid}} = \frac{\sum_f (2f+1) E_{n\ell j f}}{\sum_f (2f+1)} \quad (30)$$

and the fine-structure centroid is defined as

$$E_{n\ell}^{\text{centroid}} = \frac{\sum_j (2j+1) E_{n\ell j}^{\text{centroid}}}{\sum_j (2j+1)}. \quad (31)$$

IV. DISCUSSION

Here we have presented a simple fitting formula and parameters, equation (4) and Tables I, and V through VIII, that are sufficient to reproduce all hyperfine energy levels of hydrogen up to $\ell = 30$. The theoretical uncertainty of any level is given by equation (21) and additional systematic shifts in those levels due to a proton

these parameters should not be viewed as fundamental, but a given set of them have a practical use in reproducing theoretical energy levels without having to use the QED theory directly. When using these parameters, only the values from a single fit should be used. Furthermore, all reported digits of the parameters up to an absolute precision of 10^{-15} should conservatively be used to reproduce the levels below the theoretical uncertainty (21).

Following the same rationale leading to equation (21), the theoretical error for any given transition is

$$\delta(\nu(n_i \ell_i \rightarrow n_f \ell_f)) = \left| 1.9 \text{ kHz} \left(\frac{\delta_{\ell_f,0}}{n_f^3} - \frac{\delta_{\ell_i,0}}{n_i^3} \right) - 2.2 \text{ kHz} \left(\frac{1}{n_f^2} - \frac{1}{n_i^2} \right) \right|, \quad (32)$$

whereas the shift in a transition due to a shift in the proton radius can be easily computed using (24).

In some cases the measurement and theory (columns 2 and 5 of Table IV) disagree. However, the sums of values in columns 5 and 6 are in good agreement with the measured values in column 2, which confirms that these disagreements are still well characterized by shifts in the proton radius.

radius that differs from the one determined by Antognini et al. [14] is parameterized in equation (24).

Acknowledgements

We greatly appreciate the initial suggestion of Eric Hessels to pursue this work.

Interval	Measurement [kHz]	Inferred r_p [fm]	Ref.	This work [kHz]	$\Delta(\nu)_{r_p}$ [kHz]
$\nu(1S_{1/2}^{(f=1)} \rightarrow 3S_{1/2}^{(f=1)})$	2 922 742 936 722.4(2.6)	0.877(13)	[5]	2 922 742 936 715.3(1)	+7.1
	2 922 742 936 716.72(72)	0.8482(38)	[21]	2 922 742 936 715.3(1)	+1.4
$\nu(2S_{1/2}^{(f=0)} \rightarrow 2P_{1/2}^{(f=1)})$	909 871.7(3.2)	0.833(10)	[22]	909 874.1(2)	-2.6
$\nu(2S \rightarrow 4P)_{\text{FS centroid}}$	616 520 931 626.8(3.3)	0.8335(95)	[23]	616 520 931 628.6(2)	-1.9
$\nu(2S_{1/2} \rightarrow 8D_{5/2})_{\text{HFS centroid}}$	770 649 561 570.9(2.0)	0.8584(51)	[6]	770 649 561 564.0(3)	+6.8

TABLE IV: A selection of recently measured frequency (energy) intervals of hydrogen and the proton radius values inferred from them in columns 2 and 3, respectively; in column 5 are the bound-state QED predictions using the fitting formula (4) and defect parameters in Tables I and V, which are based on $r_p = 0.84087(39)$ fm; in column 6 are the proton radius corrections to column 5 using the proton radius from column 3, according to equation (24).

-
- [1] M. S. Safronova, D. Budker, D. DeMille, D. F. J. Kimball, A. Derevianko, and C. W. Clark, *Rev. Mod. Phys.* **90**, 025008 (2018), 1710.01833.
- [2] R. Pohl, A. Antognini, F. Nez, F. D. Amaro, F. Biraben, et al., *Nature* **466**, 213 (2010).
- [3] P. J. Mohr, B. N. Taylor, and D. B. Newell, *Rev. Mod. Phys.* **84**, 1527 (2012), URL <https://link.aps.org/doi/10.1103/RevModPhys.84.1527>.
- [4] W. Ubachs, *Science* **370**, 1033 (2020).
- [5] H. Fleurbaey, S. Galtier, S. Thomas, M. Bonnaud, L. Julien, F. Biraben, F. Nez, M. Abgrall, and J. Guéna, *Physical review letters* **120**, 183001 (2018).
- [6] A. D. Brandt, S. F. Cooper, C. Rasor, Z. Burkley, A. Matveev, and D. C. Yost, *Phys. Rev. Lett.* **128**, 023001 (2022), 2111.08554.
- [7] P. Yzombard, S. Thomas, L. Julien, F. Biraben, and F. Nez, *The European Physical Journal D* **77**, 23 (2023).
- [8] E. Tiesinga, P. J. Mohr, D. B. Newell, and B. N. Taylor, *Rev. Mod. Phys.* **93**, 025010 (2021).
- [9] D. M. Jacobs, *Phys. Rev. A* **106**, 062810 (2022), 2206.02494.
- [10] X. Fan, T. G. Myers, B. A. D. Sukra, and G. Gabrielse, *Phys. Rev. Lett.* **130**, 071801 (2023), URL <https://link.aps.org/doi/10.1103/PhysRevLett.130.071801>.
- [11] S. Patra, M. Germann, J. P. Karr, M. Haidar, L. Hilico, V. I. Korobov, F. M. J. Cozijn, K. S.E. Eikema, W. Ubachs, and J. C. J. Koelemeij, *Science* **369**, 1238 (2020), 2204.10674.
- [12] S. Alighanbari, G. Giri, F. L. Constantin, V. Korobov, and S. Schiller, *Nature* **581**, 152 (2020).
- [13] D. J. Fink and E. G. Myers, *Physical Review Letters* **124**, 013001 (2020).
- [14] A. Antognini, F. Nez, K. Schuhmann, F. D. Amaro, F. Biraben, et al., *Science* **339**, 417 (2013).
- [15] M. Horbatsch and E. A. Hessels, *Physical Review A* **93**, 022513 (2016).
- [16] S. G. Karshenboim, *Physics reports* **422**, 1 (2005).
- [17] N. Kolachevsky, A. Matveev, J. Alnis, C. G. Parthey, S. G. Karshenboim, and T. W. Hänsch, *Physical Review Letters* **102**, 213002 (2009).
- [18] C. G. Parthey, A. Matveev, J. Alnis, B. Bernhardt, A. Beyer, R. Holzwarth, et al., *Phys.Rev.Lett.* **107**, 203001 (2011), 1107.3101.
- [19] G. W. F. Drake and R. A. Swainson, *Phys. Rev. A* **41**, 1243 (1990).
- [20] U. D. Jentschura and P. J. Mohr, *Physical Review A* **72**, 012110 (2005).
- [21] A. Grinin, A. Matveev, D. C. Yost, L. Maisenbacher, V. Wirthl, R. Pohl, T. W. Hänsch, and T. Udem, *Science* **370**, 1061 (2020).
- [22] N. Bezginov, T. Valdez, M. Horbatsch, A. Marsman, A. C. Vutha, and E. A. Hessels, *Science* **365**, 1007 (2019).
- [23] A. Beyer, L. Maisenbacher, A. Matveev, R. Pohl, K. Khabarova, A. Grinin, T. Lamour, D. C. Yost, T. W. Hänsch, N. Kolachevsky, et al., *Science* **358**, 79 (2017).

Appendix A: Fit parameters for $\ell = 2$ through $\ell = 30$

ℓ	j	f	δ_i	Value/ 10^{-5}
2	$\frac{3}{2}$	1	δ_0	1.332 822 5338
			δ_2	0.001 348 0751
			δ_4	-0.015 166 1825
			δ_6	0.142 299 3047
			δ_8	-0.533 020 4369
2	$\frac{3}{2}$	2	δ_0	1.331 095 4021
			δ_2	0.001 348 1369
			δ_4	-0.015 166 1916
			δ_6	0.142 299 4035
			δ_8	-0.533 020 8355
2	$\frac{5}{2}$	2	δ_0	0.887 597 5544
			δ_2	0.001 348 2663
			δ_4	-0.015 171 2667
			δ_6	0.142 369 4195
			δ_8	-0.533 332 7777
2	$\frac{5}{2}$	3	δ_0	0.886 487 6120
			δ_2	0.001 348 2916
			δ_4	-0.015 171 2659
			δ_6	0.142 369 4111
			δ_8	-0.533 332 7469
3	$\frac{5}{2}$	2	δ_0	0.888 222 9673
			δ_2	0.000 781 8922
			δ_4	-0.008 421 7392
			δ_6	0.053 242 8585
			δ_8	0.053 242 8585
3	$\frac{5}{2}$	3	δ_0	0.887 429 9452
			δ_2	0.000 781 9176
			δ_4	-0.008 421 7409
			δ_6	0.053 242 8702
			δ_8	0.053 242 8702
3	$\frac{7}{2}$	3	δ_0	0.665 695 0501
			δ_2	0.000 781 9366
			δ_4	-0.008 422 7940
			δ_6	0.053 250 0463
			δ_8	0.053 250 0463
3	$\frac{7}{2}$	4	δ_0	0.665 107 7533
			δ_2	0.000 781 9505
			δ_4	-0.008 422 7940
			δ_6	0.053 250 0464
			δ_8	0.053 250 0464
4	$\frac{7}{2}$	3	δ_0	0.666 044 8195
			δ_2	0.000 462 1199
			δ_4	-0.003 176 3090
4	$\frac{7}{2}$	4	δ_0	0.665 587 9476
			δ_2	0.000 462 1338
			δ_4	-0.003 176 3094
4	$\frac{9}{2}$	4	δ_0	0.532 550 4600
			δ_2	0.000 462 1300
			δ_4	-0.003 176 5643
4	$\frac{9}{2}$	5	δ_0	0.532 187 0988
			δ_2	0.000 462 1388
			δ_4	-0.003 176 5643

TABLE V: Same as Table I, but for $\ell = 2 - 4$ channels.

ℓ	j	f	δ_i	Value/ 10^{-6}
5	$\frac{9}{2}$	4	δ_0	5.327 754 771
			δ_2	0.003 595 064
			δ_4	-0.033 558 712
5	$\frac{9}{2}$	5	δ_0	5.324 781 378
			δ_2	0.003 595 152
			δ_4	-0.033 558 714
5	$\frac{11}{2}$	5	δ_0	4.437 876 418
			δ_2	0.003 595 111
			δ_4	-0.033 560 844
5	$\frac{11}{2}$	6	δ_0	4.435 406 543
			δ_2	0.003 595 172
			δ_4	-0.033 560 844
6	$\frac{11}{2}$	5	δ_0	4.439 458 289
			δ_2	0.002 004 614
6	$\frac{11}{2}$	6	δ_0	4.437 368 141
			δ_2	0.002 004 674
6	$\frac{13}{2}$	6	δ_0	3.803 869 369
			δ_2	0.002 004 589
6	$\frac{13}{2}$	7	δ_0	3.802 081 331
			δ_2	0.002 004 634
7	$\frac{13}{2}$	6	δ_0	3.805 036 168
			δ_2	0.001 679 042
7	$\frac{13}{2}$	7	δ_0	3.803 486 374
			δ_2	0.001 679 086
7	$\frac{15}{2}$	7	δ_0	3.328 364 540
			δ_2	0.001 679 019
7	$\frac{15}{2}$	8	δ_0	3.327 010 229
			δ_2	0.001 679 053
8	$\frac{15}{2}$	7	δ_0	3.329 264 456
			δ_2	0.001 433 670
8	$\frac{15}{2}$	8	δ_0	3.328 069 368
			δ_2	0.001 433 704
8	$\frac{17}{2}$	8	δ_0	2.958 531 330
			δ_2	0.001 433 650
8	$\frac{17}{2}$	9	δ_0	2.957 469 992
			δ_2	0.001 433 677
9	$\frac{17}{2}$	8	δ_0	2.959 246 785
			δ_2	0.001 242 839
9	$\frac{17}{2}$	9	δ_0	2.958 297 092
			δ_2	0.001 242 865
9	$\frac{19}{2}$	9	δ_0	2.662 667 315
			δ_2	0.001 242 821
9	$\frac{19}{2}$	10	δ_0	2.661 813 158
			δ_2	0.001 242 843
10	$\frac{19}{2}$	9	δ_0	2.663 256 892
10	$\frac{19}{2}$	10	δ_0	2.662 484 028
10	$\frac{21}{2}$	10	δ_0	2.420 605 509
10	$\frac{21}{2}$	11	δ_0	2.419 903 259

TABLE VI: Same as Table I, but for $\ell = 5 - 10$ channels.

ℓ	j	f	$\delta_0/10^{-6}$
11	$\frac{21}{2}$	10	2.421 087 670
11	$\frac{21}{2}$	11	2.420 446 444
11	$\frac{23}{2}$	11	2.218 881 255
11	$\frac{23}{2}$	12	2.218 293 695
12	$\frac{23}{2}$	11	2.219 288 139
12	$\frac{23}{2}$	12	2.218 747 551
12	$\frac{25}{2}$	12	2.048 192 551
12	$\frac{25}{2}$	13	2.047 693 703
13	$\frac{25}{2}$	12	2.048 540 521
13	$\frac{25}{2}$	13	2.048 078 600
13	$\frac{27}{2}$	13	1.901 888 706
13	$\frac{27}{2}$	14	1.901 459 890
14	$\frac{27}{2}$	13	1.902 189 702
14	$\frac{27}{2}$	14	1.901 790 439
14	$\frac{29}{2}$	14	1.775 092 605
14	$\frac{29}{2}$	15	1.774 720 039
15	$\frac{29}{2}$	14	1.775 355 379
15	$\frac{29}{2}$	15	1.775 006 833
15	$\frac{31}{2}$	15	1.664 146 281
15	$\frac{31}{2}$	16	1.663 819 578
16	$\frac{31}{2}$	15	1.664 377 841
16	$\frac{31}{2}$	16	1.664 070 924
16	$\frac{33}{2}$	16	1.566 252 829
16	$\frac{33}{2}$	17	1.565 964 011
17	$\frac{33}{2}$	16	1.566 458 423
17	$\frac{33}{2}$	17	1.566 186 098
17	$\frac{35}{2}$	17	1.479 236 708
17	$\frac{35}{2}$	18	1.478 979 546
18	$\frac{35}{2}$	17	1.479 420 472
18	$\frac{35}{2}$	18	1.479 177 201
18	$\frac{37}{2}$	18	1.401 380 310
18	$\frac{37}{2}$	19	1.401 149 960
19	$\frac{37}{2}$	18	1.401 545 635
19	$\frac{37}{2}$	19	1.401 327 005
19	$\frac{39}{2}$	19	1.331 309 900
19	$\frac{39}{2}$	20	1.331 102 223
20	$\frac{39}{2}$	19	1.331 459 274
20	$\frac{39}{2}$	20	1.331 261 721
20	$\frac{41}{2}$	20	1.267 912 924
20	$\frac{41}{2}$	21	1.267 724 795

TABLE VII: Same as Table I, but for $\ell = 11 - 20$ channels.

ℓ	j	f	$\delta_0/10^{-6}$
21	$\frac{41}{2}$	20	1.268 048 616
21	$\frac{41}{2}$	21	1.267 869 232
21	$\frac{43}{2}$	21	1.210 279 427
21	$\frac{43}{2}$	22	1.210 108 210
22	$\frac{43}{2}$	21	1.210 403 234
22	$\frac{43}{2}$	22	1.210 239 622
22	$\frac{45}{2}$	22	1.157 657 634
22	$\frac{45}{2}$	23	1.157 501 147
23	$\frac{45}{2}$	22	1.157 771 053
23	$\frac{45}{2}$	23	1.157 621 220
23	$\frac{47}{2}$	23	1.109 421 071
23	$\frac{47}{2}$	24	1.109 277 491
24	$\frac{47}{2}$	23	1.109 525 356
24	$\frac{47}{2}$	24	1.109 387 632
24	$\frac{49}{2}$	24	1.065 043 500
24	$\frac{49}{2}$	25	1.064 911 294
25	$\frac{49}{2}$	24	1.065 139 712
25	$\frac{49}{2}$	25	1.065 012 686
25	$\frac{51}{2}$	25	1.024 079 646
25	$\frac{51}{2}$	26	1.023 957 513
26	$\frac{51}{2}$	25	1.024 168 686
26	$\frac{51}{2}$	26	1.024 051 159
26	$\frac{53}{2}$	26	0.986 150 199
26	$\frac{53}{2}$	27	0.986 037 031
27	$\frac{53}{2}$	26	0.986 232 841
27	$\frac{53}{2}$	27	0.986 123 786
27	$\frac{55}{2}$	27	0.950 930 040
27	$\frac{55}{2}$	28	0.950 824 884
28	$\frac{55}{2}$	27	0.951 006 950
28	$\frac{55}{2}$	28	0.950 905 481
28	$\frac{57}{2}$	28	0.918 138 893
28	$\frac{57}{2}$	29	0.918 040 928
29	$\frac{57}{2}$	28	0.918 210 647
29	$\frac{57}{2}$	29	0.918 116 000
29	$\frac{59}{2}$	29	0.887 533 853
29	$\frac{59}{2}$	30	0.887 442 365
30	$\frac{59}{2}$	29	0.887 600 953
30	$\frac{59}{2}$	30	0.887 512 463
30	$\frac{61}{2}$	30	0.858 903 359
30	$\frac{61}{2}$	31	0.858 817 727

TABLE VIII: Same as Table I, but for $\ell = 21 - 30$ channels.